Rational design of highly dispersed Fe-N-C based on 1,10phenanthroline-2,9-dicarboxylic acid as preorganized ligand for precursor: boosted electrochemiluminescence detection of tetracycline

Li-Ping Zong, Junji Li, Guofang Shu, Xinye Liu, Robert Marks, Xue-Ji Zhang, Serge Cosnier, Dan Shan

Rational design of highly dispersed Fe-N-C based on 1,10-phenanthroline-2,9-dicarboxylic acid as preorganized ligand for precursor: boosted electrochemiluminescence detection of tetracycline

Journal:	*Analytical Chemistry*
Manuscript ID	ac-2021-045587
Manuscript Type:	Article
Date Submitted by the Author:	21-Oct-2021
Complete List of Authors:	Zong, Li-Ping; Nanjing University of Science and Technology, School of Environmental and Biological Engineering Li, Junji; Nanjing University of Science and Technology, School of Environmental & Biological Engineering Shu, Guofang; Southeast University Zhongda Hospital Marks, Robert; Ben-Gurion University of the Negev, Department of Biotechnology Engineering Zhang, Xueji; University of Science and Technology Beijing, Research Center for Bioengineering & Sensing Technology Cosnier, Serge; Universite Grenoble Alpes, Département de Chimie Moléculaire UMR CNRS 5250 Shan, Dan; Nanjing University of Science and Technology, School of Environmental and Biological Engineering

Rational design of highly dispersed Fe-N-C based on 1,10-phenanthroline-2,9-dicarboxylic acid as preorganized ligand for precursor: boosted electrochemiluminescence detection of tetracycline

Li-Ping Zong[a], Junji Li[a], Guofang Shu[b], Xinye Liu, Robert-S. Marks[c], Xue-Ji Zhang[a,d], Serge Cosnier[e], Dan Shan[a]*

[a] School of Environmental and Biological Engineering, Nanjing University of Science and Technology, Nanjing 210094, P R China

[b] Department of Clinical Laboratory, Zhongda Hospital, Southeast University School of Medicine, Nanjing 210009, P R China

[c] Department of Biotechnology Engineering, Ben-Gurion University of the Negev, Beer-Sheva, Israel

[d] School of Biomedical Engineering, Health Science Centre, Shenzhen University, Shenzhen 518060, P R China

[e] University of Grenoble Alpes-CNRS, DCM UMR 5250, F-38000 Grenoble, France

* Corresponding author:
E-mail: (D. Shan)

ABSTRACT: In view of the shortcomings of the current coreactant electrochemiluminescence (ECL) and inspired by natural oxygen (O_2) reduction metalloenzymes, a novel ECL amplification strategy was established. A pyrolytic iron and nitrogen-doped (Fe-N-C) material rich in $V_O^{\bullet}$ defects was rationally designed by destroying the highly saturated coordination with preorganized ligand PDA. Extraordinary catalytic activity for O_2 activation was obtained *via* screening a special pyrolysis temperature using spectroscopic and electrochemical methods. The high-spin ferric centers of highly dispersed FeC nanoclusters, abundant carbon and oxygen vacancy defects, fully contributed to the inherent catalytic activity. ECL amplification was achieved by integrating the material with luminol to generate redox active radicals *in situ* from dissolved O_2 and simultaneously shorten the transferring distance of radicals. Tetracycline (TC), which posed a growing threat to aquatic biodiversity and environmental safety, as the model antibiotic was successfully detected with a detection limit of 3.88 nM (S/N = 3), clarifying a promising application prospect of this new effective ECL amplification strategy in biological analysis and environmental monitoring.

KEYWORDS: 1,10-phenanthroline-2,9-dicarboxylic acid (PDA), *in situ* generated coreactant, electrochemiluminescence (ECL), tetracycline

Tetracycline (TC), a representative antibiotic, has brought obvious problems to environmental safety and human health due to the abuse of antibiotics in aquaculture, livestock husbandry and human disease prevention.[1] The influx of TC residues in water and soil has resulted in serious concerns, especially regarding drinking water risks and antimicrobial resistance, cause it may destroy the microbial ecological structure in aquatic environment and pose a serious threat to human beings. Long-term exposure of TC to the human body can cause allergic reactions, gastrointestinal disorders, hepatotoxicity, etc. Therefore, it is of paramount importance to develop a simple, rapid and low-cost sensor for monitoring TC pollution in water samples.

Electrochemiluminescence (ECL), as an analytical method with the virtues of high sensitivity, low background, wide dynamic range, good time and space control over light emission and simple equipment requirement, has been widely applied in the fields of disease diagnosis, food safety testing, and environmental monitoring. ECL mechanism is mainly divided into annihilation and coreaction mechanism. Though the coreactant system has been extensively studied due to the relatively high ECL efficiency and the lack of potential cycle scanning compared with annihilation system. The coreactant systems still have some shortcomings, such as transporting coreactant to emitter, short lifetime of radicals and interference with the stability of analytes. For example, the self-decomposition of H_2O_2 in luminol-H_2O_2 system would affect the application in quantitative analysis and H_2O_2 may oxidize or reduce analytes. Therefore, it is very desirable to construct a ECL system with virtues of both high luminous efficiency and coreactant interference-free.

A promising approach is *in situ* generation of coreactant from dissolved oxygen (O_2) in the electrolyte. Notably, many of the O_2 reduction enzymes in nature are iron dependent, such as cytochromes P450 (P450), Rieske dioxygenase, Cysteine dioxygenase. And the metalloenzymes incorporate O atom into substrates in (di)oxygenases or reduce molecular O_2 to H_2O in oxidases through the activation of O_2 to generate high-valent metal-oxo intermediates.[2] What's more, non-heme high-valent Fe complexes with terminal oxygen structures

have been confirmed to be the reaction core of ferritin involved in O_2 activation.[3] Motivated by this, we come up with the idea of amplifying ECL by directly reducing dissolved O_2 to reactive oxygen species (ROS) as coreactant. Generating coreactant *in situ* shall shorten the transferring distance of radicals and thereby drastically enhance the luminous efficiency. Compared with the fragility and instability of natural metalloenzymes, the biomimetic studies of mimic enzymes can provide us with an alternative and facile strategy. Fe-N, and Fe-O bonds in Fe- and N-doped materials have been proved to greatly contribute to catalytic activity of oxygen reduction reaction (ORR) electrocatalysts.[4-6] And inspired by the natural dioxygenases and oxidases, we are desired to construct an oxidase analogue electrocatalyst consisting of Fe complexes with terminal oxygen structures to activate O_2. Therefore, rational choice of bridging ligand to build unsaturated Fe center in coordination with N and O atoms is extremely needed. 1,10-phenanthroline-2,9-dicarboxylic acid (PDA) is based on the rigid phenanthroline skeleton with donor groups at the 2- and 9-positions. The two carboxylic acid groups at the 2- and 9-positions of PDA are strongly constrained to remain nearly coplanar with the phenanthroline moiety,[7] which is very beneficial for the formation of a planar metal catalytic center with strong catalytic properties. On the other hand, we supposed that the complex of Fe and PDA can achieve excellent dispersion of Fe atoms due to the formation of three rigid five-membered chelate rings upon coordination.

Therefore, in this work, the rigid and highly preorganized ligand PDA was adopted to construct a precursor of highly efficient electrocatalyst for O_2 activation. The precursor was pyrolyzed to fabricate iron- and nitrogen-doped materials. The pyrolysis temperature was precisely adjusted to regulate the intrinsic electrocatalytic activity and to find a balance fitting in the luminol ECL system. Gradually, an ECL amplification strategy was designed based on the Fe-N-C/luminol modified electrodes *via* directly generating redox free radicals *in situ*. TC antibiotic was used as the analyte to evaluate the performance of the proposed ECL immunosensor.

■ Experimental section

Materials and Reagents. All reagents were commercially available and used without further pretreatments or purifications. 1,10-phenanthroline-2,9-dicarboxylic acid (PDA), ferric nitrate nonahydrate ($Fe(NO_3)_3{\cdot}9H_2O$), luminol and tetracycline (TC) were purchased from Aladdin Biochemical Technology Co., Ltd. (Shanghai, China). Luminol (3-aminophthalhydrazide) stock solution (0.01 M) was prepared in a 0.1 M NaOH solution and stored in a 4 ℃ refrigerator for at least 2 weeks before use. All aqueous solutions were prepared with deionized water obtained from a Millipore water purification system (≥18 MΩ, Milli-Q, Millipore).

Apparatus. Ultraviolet-vis (UV-Vis) spectra were recorded on the Shimadzu UV-3600 spectrophotometer. Fourier-transformation infrared (FT-IR) spectra were obtained with an IR-Prestige-21 FT-IR spectrometer (Shimadzu Co., Japan). Thermal gravimetric analysis and differential scanning calorimetry (TG-DSC) was investigated on Synchro Thermal Analyzer (STA 449 F1 Jupiter. NETZSCH). X-ray diffraction (XRD) patterns were collected on X-ray diffractometer (Bruker D8) at 40 kV and 40 mA. Raman spectra were obtained with iHR550 Raman microscope (HORIBA scientific) with 532 nm solid laser as excitation source. The morphology was investigated with a XL-30E scanning electron microscope (SEM). X-ray photoelectron spectroscopy (XPS) were obtained with K-Alpha (Thermo Fisher Scientific Co., USA). Electron paramagnetic resonance (EPR) was performed on Bruker spectrometer (E500, Bruker Instrument, Germany). Electrochemical impedance spectroscopy (EIS) was investigated on Autolab PGSTAT30 (Eco Chemie) controlled by NOVA 1.10 software. Electrochemical measurements were investigated on CHI 660D electrochemical workstation (Chenhua, China). ECL was investigated on MPI-EII multifunctional electrochemical and chemiluminescent analytical system (Xi'an Remex Analytical Instrument Co., Ltd, China).

Methods. Preparation of the catalyst Fe-N-C. The precursor was obtained according to a typical one-step synthesis. 10 mM $Fe(NO_3)_3{\cdot}9H_2O$ and 20 mM PDA were dissolved respectively in 10.0 mL methanol by ultrasonic treatment, called as solution A and solution B. Then solution A was added dropwise into the solution B under stirring. The mixture was stirred vigorously for 3h at room temperature. Afterward, the precursor FePDA was gathered by centrifugation (8000 rpm), washed three times with methanol and freeze-dried overnight in a vacuum. Finally, the product termed Fe-N-C-X (X=400, 500, 600, 700, 800, 900℃) was obtained by pyrolysis in a N_2 atmosphere at corresponding temperature for 2 h, with a heating rate of 3℃ min^{-1}.

Electrochemical measurements. A conventional three-electrode cell was employed. For cyclic voltammetry (CV) and linear sweep voltammetry (LSV), a rotating disk electrode (RDE, 5 mm in diameter) as working electrode, a saturated calomel Hg/Hg_2Cl_2 electrode as reference electrode, a graphite rod as counter electrode. The electrode was sufficiently polished with 0.3 and 0.05 μm alumina powder and rinsed by deionized water for further use. A flow of N_2 or O_2 was maintained over the electrolyte for continuous N_2 or O_2 saturation during electrochemical measurements. To obtain Fe-N-C/RDE, 20 μL 5 mg mL^{-1} Fe-N-C suspension in water was dripped on the pretreated RDE, followed by 10 μL 0.5wt% nafion/ethanol solution, and dried in air. All the potentials were converted to reversible hydrogen electrode (RHE), E (RHE) = E (Hg/Hg_2Cl_2) + 1.008 V.

ECL detection of TC. For ECL measurements, a glassy carbon electrode (GCE, 5 mm in diameter) as working electrode, an Ag/AgCl electrode as reference electrode, a Pt wire as counter electrode. 10 μL 2 mg mL^{-1} Fe-N-C suspension in water and 10 μL 10 mM luminol solution were pre-mixed by ultrasonic treatment and then dripped on the surface of GCE, followed by 10 μL 0.5 wt% nafion/ethanol solution, and lastly dried in darkness at room temperature to obtain GCE/Fe-N-C/luminol. PBS containing different concentration of TC was prepared as working electrolyte. The modified GCE was immersed in the electrolyte for about 5 min before ECL measurement started. The photomultiplier tube was set at 1000 V and the magnification level was fixed at 2 for ECL measurements.

■ RESULTS

Electrochemical investigation. As mentioned above, the oxygen reduction activity of the catalyst was assessed using the RDE technique. As shown in the CV curves of FePDA and Fe-N-C-800 (Fig. 1A, B), the potential of cathodic peak (E_{pc}) of Fe-N-C-800 was 0.90 V vs. RHE, much more positive than

0.59 V of FePDA at O_2 saturated atmosphere. And large difference of cathodic peak currents (DI) was observed and calculated as 0.75 mA cm^{-2}. The electron transfer number (n) of Fe-N-C-800 in 0.1 M, pH 11 PBS was calculated as 3.18 according to the RDE voltammograms as shown in Fig. S1.

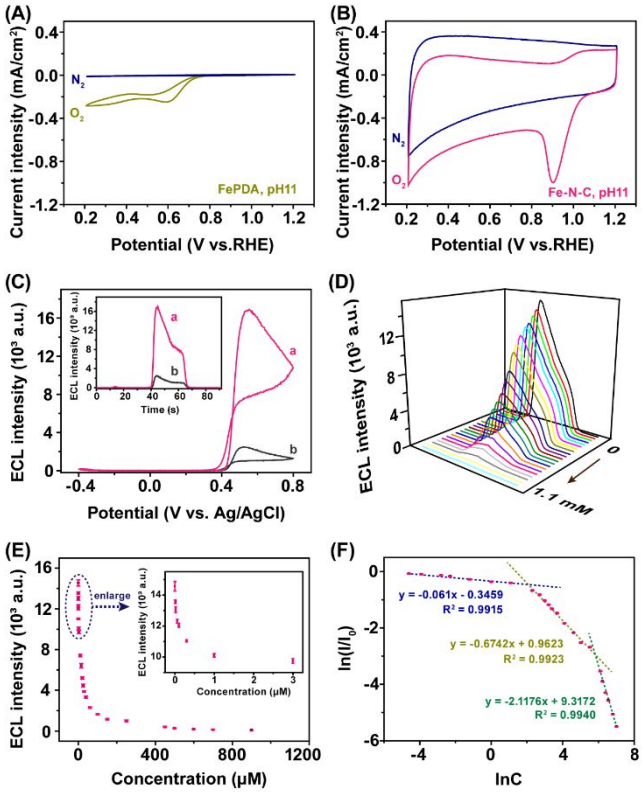

Figure 1 CV curves of (**A**) FePDA and (**B**) Fe-N-C-800 in N_2 and O_2 saturated 0.1 M, pH 11 PBS, scan rate: 10 mV s^{-1}. (**C**) ECL-potential curves of Fe-N-C-800/luminol/GCE and luminol/GCE in O_2 saturated 0.1 M, pH 7.4 PBS during a cycle scan from -0.4 to 0.8 V, scan rate: 30 mV s^{-1}. **Inset C**: Corresponding ECL-time curves. (**D**) ECL-time curves of Fe-N-C-800/luminol/GCE at different concentrations of TC (0.02, 0.06, 0.1, 0.3, 1, 3, 10, 15, 20, 25, 30, 40, 60, 100, 150, 250, 450, 700, 1100 μM) in 0.1 M, pH 11 PBS during a cycle scan from 0 to -0.4 to 0.8 V, scan rate: 100 mV s^{-1}. (**E**) ECL intensity versus TC concentration. Error bars, SD, n = 3. **Inset E**: Enlarged graph. (**F**) The calibration plot of $\ln(I/I_0)$ (the natural logarithm of ratio of I to I_0, I and I_0 represent ECL peak intensity with and without TC) versus lnC (the natural logarithm of TC concentration). Error bars, SD, n = 3.

ECL response. At the beginning, the ECL behaviors of the Fe-N-C/luminol were investigated in 0.1 M, pH 7.4 PBS within the scan range of -0.4 to 0.8 V. As observed from Fig. 1C, the ECL intensity of Fe-N-C-800/luminol/GCE was almost 10-fold enhanced compared with that of luminol/GCE under O_2 saturated atmosphere. As displayed in Fig. S2, the stability of the enhancement of Fe-N-C-800 on ECL was also studied. The ECL response of Fe-N-C-800/luminol/GCE was observed with relative standard deviation (RSD) of 0.16% upon 20 cycles of continuous scans.

ECL detection of TC. Accidentally we found that the addition of tetracycline (TC) could effectively quench the ECL of Fe-N-C-800/luminol/GCE. The optimal condition was determined prior to detection. The low and initial potential were optimized, setting a comparatively narrow potential scanning window from 0 V to -0.4 V to 0.8 V. The optimal pH for ECL of Fe-N-C/luminol turned out to be 11 (Fig. S3A), different from the optimal pH value of 13 for O_2 reduction (Fig. S1B, C). The electrode capacity of catalyst and the luminol concentration had also been optimized (Fig. S3B, C). A capacity of 25.46 μg cm^{-2} Fe-N-C and 5 mM luminol demonstrated the best ECL performance.

Under the optimal condition, quantitative analysis of TC was conducted. Notably, TC aqueous solution should always be protected from light. Fig. 1D presented the ECL-time curves recorded under different TC concentration. ECL peak intensity decreased with the increase of TC concentration as shown in Fig. 1E. Three good linear segments were observed and the linear regression equations were fitted as shown in Fig. 1F. The limit of detection (LOD) was estimated as 3.88 nM according to the reported calculation method.[1] According to signal-to-noise ratio of 3 (n), The lowest detection signal $I_L = I_B - S_B$ n = 14924.90-155.40*3 = 14458.70, I_0 = 14565.06. Then substitute I_L and I_0 into the linear equation. The LOD value was lower than the MRLs of 676 nM and 225 nM TC in milk set by the U.S. FDA and EU, respectively.[2] As shown in Table S1, the proposed sensor displayed wider detection range and comparatively high sensitivity compared with other reported ECL, colorimetry and fluorescent sensors.

The ECL potential cycling stability, long-term stability, and selectivity of the sensor were further evaluated. The ECL response was observed with RSD of 1.41% upon 25 cycles of continuous cyclic scans (Fig. S4A). The ECL response under the same condition was detected at one-day interval for 11 days, which only slightly decreased after six tests with RSD of 2.05% (Fig. S4B). As shown in Fig. S4C, the ECL intensity of interfering substance was similar to that of blank, only the addition of 25 μM TC resulted in drastically dropping signal.

The practicability of the ECL sensor for water sample detection was further evaluated through recovery experiments with standard additions in actual river water and pure milk samples. Table S2 presented the feasible experimental results, calculated recovery rate and RSD.

■ DISCUSSION

Choice of PDA as the bridging ligand to build unsaturated Fe center in coordination with N and O atoms was exactly rational, in terms of its highly preorganized structure with nearly coplanar donor groups constrained to the rigid phenanthroline skeleton. Fe^{3+} was selected rather than the unstable Fe^{2+} to participate in the coordination for the accuracy and simplicity of experimental operation. The structural formula of the compound was inferred as $[Fe(PDA(H_{0.50}))(H_2O)_3](NO_3)_{1.50}$ based on the experiments and literature research, the coordination mode of the too small Fe^{3+} was possibly seven-coordinate instead of usual six to accommodate the size preference of the ligand for larger metal ion.[3-5] This perfect saturated coordination structure would be robust and therefore cannot be acting as the catalytically active site.[6-8] On this basis, it was necessary to break the saturated coordination environment of Fe in correlation with an increased catalytic activity, a promising way in this work was through high-temperature pyrolysis. A typical pyrolysis synthesis process was illustrated in Scheme 1.

Scheme 1. Schematic illustration of preparation process of the Fe-N-C/luminol.

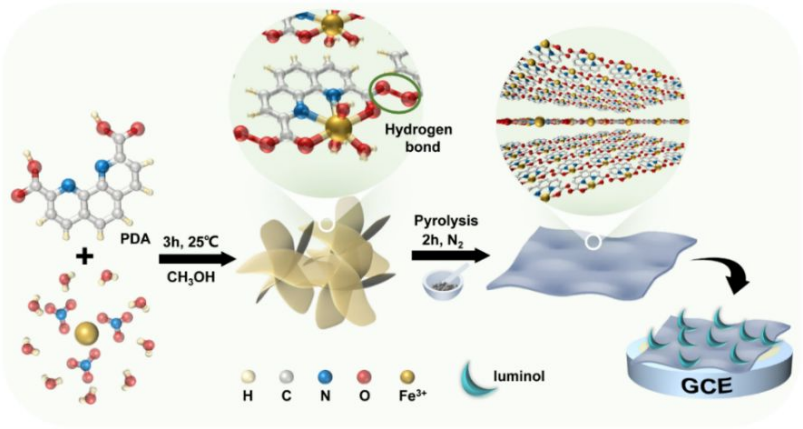

Firstly, the coordination mode of precursor FePDA was confirmed by Fourier-transformation infrared (FT-IR) in Fig. 2A. The absorbance bands for carboxylic groups of PDA can be well-distinguished at the broad band around 3335 cm^{-1}, the peaks at 1719 cm^{-1} and 1225 cm^{-1} assigned to the O-H stretching vibration,[9] the C=O stretching vibration,[3,10] and the O-H bending vibration, respectively. When PDA coordinated with Fe^{3+}, the broad bands for O-H vibrations at 3335 cm^{-1} and 1225 cm^{-1} were nearly invisible. The vibrations of COO^- converted into two asymmetric stretching located at 1656 and 1575 cm^{-1}, the symmetric stretching at 1402 cm^{-1}.[3,5,11] The splitting of $n_{as}(COO^-)$ into two bands suggested that carboxylate groups were in different coordination environment.[5] The separations between $\nu_{as}(COO^-)$ and $\nu_s(COO^-)$ were 254 and 173 cm^{-1}, which were attributed to the existence of both the bridging and monodentate modes of the carboxylate groups in PDA ligands.[5] A new peak appearing at about 650 cm^{-1} was ascribed to the Fe-O stretching vibration,[12] indicating the coordination of deprotonated carboxylate groups to Fe^{3+}. Besides, the aromatic skeleton (C=N and C=C) vibrations at about 1608 and 1506 cm^{-1} of FePDA were lower shifted relative to those of PDA at about 1621 and 1556 cm^{-1}, indicating the coordination of N atoms in PDA to Fe^{3+}.[13] Moreover, weak absorption bands observed at 3070 cm^{-1} can be attributed to the C-H vibration of the aromatic groups,[11] or the coordinated H_2O in FePDA structure or an intermolecular hydrogen bond connected two carbonyl oxygen atoms of the two FePDA complexes.[3,4]. As a result, the Fe^{3+} can coordinate to all four donor atoms of PDA and water molecules.

Effects of pyrolysis. Since thermogravimetric analyses provide evidence for thermal degradation and structure elucidation of metal complexes, TG-DSC analysis were performed on FePDA under a N_2 atmosphere with a heating rate of 10℃ min^{-1}. Six main stages were exhibited in TG curves (Fig. 2B). The first weight loss of 4.04% below 290.20℃ might be due to the removal of part coordinated H_2O.[3] The second weight loss of 26.68% from 290.20 to 419.10℃ with an endothermic peak at 380.80℃ in heat flow curve might assign to the removal of the remaining H_2O and nitrate. The sum of the weight ratio of H_2O and nitrate was 30.72% close to theoretical value of 31.17% according to the inferred structural formula. The third process from 419.10 to 578.30℃, which was similar to platform with weight loss only 2.28%, might correspond to the molten state of the material. The fourth weight loss of 6.41% from 578.30 to 728.10℃ with an endothermic peak at 587.50℃ that was similar to the boiling point of PDA, might attribute to the collapse of FePDA structure and removal of part of PDA ligands.[3] The fifth weight loss of 3.79% from 728.10 to 768.10℃ with an exothermic peak at 748.50℃ might correspond to the formation of graphite carbon structure.[14] When the temperature ranged from 800 to 1000℃, there was almost no weight loss, with residual weight changing from 56.10 to 54.90%, illustrating the formation of thermally stable material.

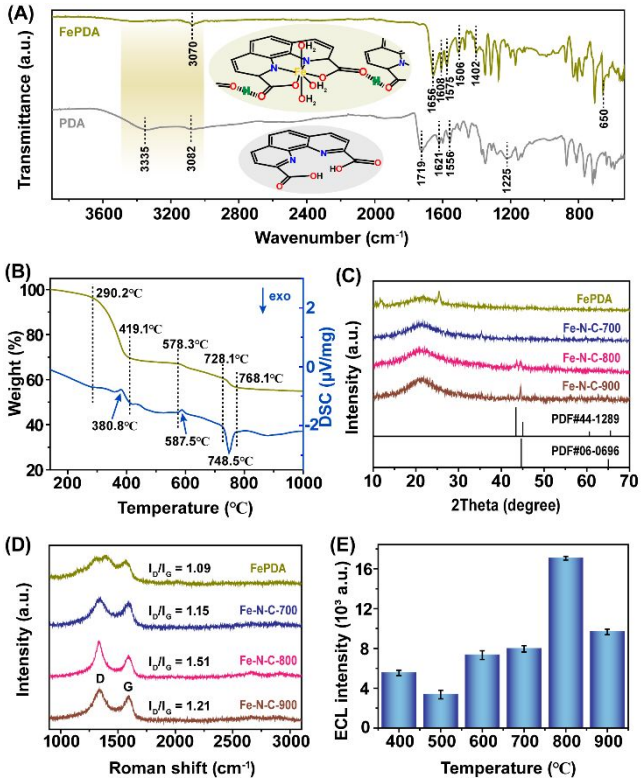

Figure 2 (**A**) Full FT-IR spectra of Fe-PDA, PDA. (**B**) TG and DSC curves of FePDA in N_2 atmosphere with a heating rate of 10℃ min^{-1}. (**C**) XRD patterns and (**D**) Roman spectra of FePDA and Fe-N-C-X (X=700, 800, 900℃) (**E**) ECL intensity versus pyrolysis temperature (Fe-N-C-X/luminol/GCE) in 0.1 M, pH 7.4 PBS under O_2 saturated atmosphere.

The influence of pyrolysis temperature was further investigated by powder X-ray diffraction (XRD) to identify the composition and crystalline nature. Compared with the material without pyrolysis, the peaks around 25° of Fe-N-C-X (X=700, 800, 900℃) became stronger and narrower (Fig. 2C), indicating that a more ordered graphite structure with stronger electronic conductivity was formed.[14] The pattern of Fe-N-C-800 showed the peak matching with $C_{0.14}Fe_{1.86}$ (PDF#44-1289). While the pattern of Fe-N-C-900 showed the peak matching with inactive Fe particles (PDF#06-0696) which did not contribute to the catalytic performance.[14] According to the Nyquist plots in Fig. S5, Fe-N-C-800 exhibited the smallest arc radius among Fe-N-C-700 and Fe-N-C-900, suggesting the strongest conductivity which was consistent with the analysis of XRD and explained the large difference of cathodic peak currents in CV curves. Furthermore, lattice disorder, defect and crystallinity of sp^2 carbon atom were evaluated by Raman spectra.[15] The calculated intensity ratios (I_D/I_G) of D band at 1337 cm^{-1} to G band at 1591 cm^{-1} was displayed in Fig. 2D. The I_D/I_G of Fe-N-C-800 (1.51) was significantly higher than that of Fe-N-C-700 (1.15) and Fe-N-C-900 (1.21). It was inferred that Fe-N-C-800 had the strongest catalytic activity since it produced the most emerging defects that were beneficial to ORR. ECL investigation was then performed to confirm this. As shown in Fig. 2E, Fe-N-C-800 induced the strongest ECL signal of luminol, confirming the effect pyrolysis brought out that pyrolysis at 800℃ gave the highest catalytic activity.

Characterization of Fe-N-C-800. More specifically, we explored the morphology and elemental composition of the optimized electrocatalyst Fe-N-C-800 firstly. The size and morphology were characterized by scanning electron microscopy (SEM) and transmission electron microscopy (TEM). FePDA was observed to distribute in butterfly-shaped flakes that crossed like butterfly wings in Fig. 3A. Fe-N-C-800 still maintained a flake-like accumulation morphology with small defects densely distributed on the surface in Fig. 3B, which may be due to the constraint from the highly preorganized ligand and π-π stacking of the phenanthroline plane skeleton. It can be seen from the TEM and HRTEM images (Fig. 3C, D, E) of Fe-N-C-800 that layered flakes were uniformly scattered with black clusters no more than 10 nm in diameter. The clearly visible lattice fringes in main part of the cluster indicated the single crystallinity. The *d*-spacing of 0.2078 nm corresponded to the (101) plane of $C_{0.14}Fe_{1.86}$, and the *d*-spacing of 0.3927 nm corresponded to the (120) plane of C, which matched the XRD pattern well. What's more, the elemental distribution densities of C, N, O, Fe were quite uniform as characterized in Fig. 3F and no obvious iron particles were observed. Once again, the dispersive restraint effect of ligand PDA was confirmed, and it was shown that a highly dispersed Fe catalyst was formed.

Secondly, localized defects, oxidation state and surrounding coordination of Fe species can be investigated through electron paramagnetic resonance (EPR) technique.[6,16] The X-band EPR spectra of FePDA and Fe-N-C-800 in Fig. 4A showed isotropic signal at g-factor of 4.01 and 8.98 corresponding to ferric high- and mid-spin states.[6,17] Interestingly, a main resonance line at magnetic field strength of 3248 G and g-factor of 2.04 can be observed, which can be attributed to the unpaired electrons trapped on oxygen vacancies (singly ionized oxygen vacancy $V_O^{\bullet}$).[16,18] Its peak intensity of Fe-N-C-800 was much higher than that of FePDA, indicating that more $V_O^{\bullet}$ defects appeared in Fe-N-C-800. In relation with their electrochemical behaviors, the amount of $V_O^{\bullet}$ defects were positively correlated to CV and ECL performance. It can be revealed that the higher the EPR peak, the more the $V_O^{\bullet}$ defects, the more positive the oxygen reduction potential and the higher the ECL response. One possible explanation was that the plenty existence of $V_O^{\bullet}$ defects improved the affinity for O_2 adsorption, which played a decisive role in the activity of electrocatalyst.[19]

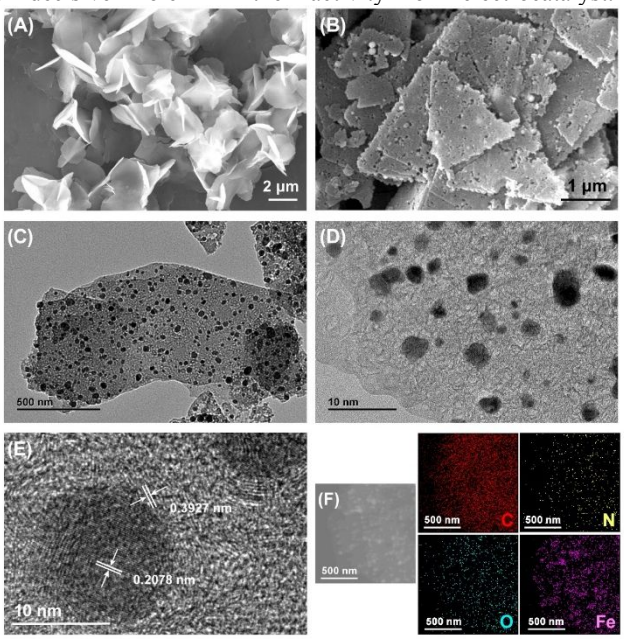

Figure 3 (**A**) SEM images of FePDA. (**B**) SEM, (**C**) TEM, (**D, E**) HRTEM, and (**F**) elemental mapping images of Fe-N-C-800.

Thirdly, the surface elemental compositions and electronic states were characterized by X-ray photoelectron spectroscopy (XPS). The full survey XPS spectra of FePDA and Fe-N-C-800 were shown in Fig. 4B. The C 1s regions (Fig. 4C) were both deconvoluted into three overlapping peaks C-C (284.8 eV), C-N (285.7 eV) and O-C=O (288.6 eV).[12] The N 1s regions (Fig. 4D) were deconvoluted into N (398.5 eV), Fe-N (399.6 eV), π-π* satellite (406.1 eV) in FePDA, and pyridinic N (398.4 eV), Fe-N (399.8 eV), graphitic N (401.6 eV), oxidized N (406.0 eV) in Fe-N-C-800, respectively.[20] The remain of Fe-N and residual N (6.47 at%) in Fe-N-C-800 shown in Table S3 further proved the firm coordination between Fe and N donors of PDA ligand. The O 1s regions (Fig. 4E) were attributed to Fe-O (529.7 eV), O=C (531.0 eV), O-C (532.1 eV), O-H (533.7 eV) in FePDA, and Fe-O (530.7 eV), O=C (531.72 eV), O-C (533.2 eV) in Fe-N-C-800, respectively.[12,21] The appearance of Fe-O further proved the coordination of Fe with COO^- and H_2O, marching well with the analysis of FT-IR. The Fe 2p regions (Fig. 4F) were fitted with Fe(II) ($2p_{3/2}$ 709.6, $2p_{1/2}$ 723.2, satellite 715.6 and 729.2 eV), Fe(III) ($2p_{3/2}$ 711, $2p_{1/2}$ 724.6, satellite 718.3 and 733.5 eV) in FePDA, and Fe(II) ($2p_{3/2}$ 710.2, $2p_{1/2}$ 723.8, satellite 713.4 and 729.0 eV), Fe(III) ($2p_{3/2}$ 711.6, $2p_{1/2}$ 725.2, satellite 718.0 and 734.0 eV) in Fe-N-C-800, respectively. The Fe(II)/Fe(III) peak area ratio of Fe-N-C-800 was obviously greater than that of FePDA, suggesting the change of coordination environment and electron density around Fe atoms with the increase of N, O content after pyrolysis.[10,22]

Furthermore, the Fe 2p orbital binding energy of Fe-N-C-800 shifted to higher position, and significant asymmetry on the main Fe $2p_{3/2}$ and Fe $2p_{1/2}$ peaks was observed, which could be attributed to multiple splitting caused by the core-hole interaction with the open-shell electronic structure of high-spin ferric centers.[23]

Based on these, the Fe-N-C-800 was characterized as a highly dispersed catalyst with high-spin ferric centers, not to mention its excellent electronic conductivity and remarkable O_2 adsorption affinity, which all greatly contributed to its catalytic activity.

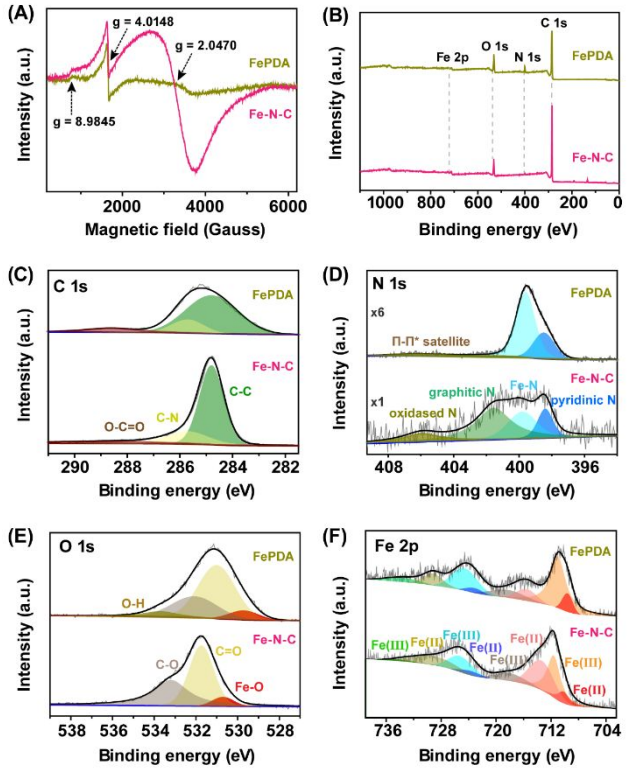

Figure 4 (**A**) Room temperature X-band EPR spectra (9.84 GHz) (modulation amplitude: 4 G / modulation frequency: 100 kHz). (**B**) Full XPS spectra and High resolution XPS spectra of (**C**) C 1s, (**D**) N 1s, (**E**) O 1s, and (**F**) Fe 2p (satellite peaks included).

ECL amplification mechanism of the Fe-N-C/luminol. Herein an ECL system with reactant generating *in situ* was successively designed, composed of luminol as the luminophore and the as-prepared Fe-N-C-800 as ECL signal amplifier. According to the Nyquist plots in Fig. S5, the semicircular diameter of Fe-N-C-800/luminol was significantly increased compared with that of Fe-N-C-800, while both of them were much smaller than the semicircular diameter of bare GCE, indicating the excellent conductivity of Fe-N-C-800 and the successful immobilization of Fe-N-C-800/luminol.

In order to reveal the ECL mechanism, the ECL behaviors of GCE/luminol/Fe-N-C-800 under different atmosphere were investigated. Fe-N-C-800/luminol/GCE tested under N_2 saturated atmosphere showed ultralow ECL response only about 400 a.u., while the ECL intensity under O_2 saturated atmosphere reached around 16000 a.u., about forty-fold increased (Fig. 5A), indicating the decisive role of dissolved O_2 in this ECL system. And the ECL intensity under air saturated atmosphere decreased slightly compared with O_2 saturated condition, confirming the necessity of O_2. Considering the oxidation luminescence mechanism of luminol and the O_2 reduction catalytic activity of Fe-N-C-800, it was proposed that various ROS were generated from dissolved O_2, and then acted as coreactant, dominantly contributing to the whole ECL process.

To further clarify the proposed mechanism, the type of ROS was identified through the study of the effects of ROS scavengers on the ECL-O_2 system (Fig. 5B). Isopropanol (IPA) and benzoquinone (BQ) were used to scavenge hydroxyl radical (•OH), and superoxide radical ($O_2^{\bullet-}$), respectively. The ECL intensity was almost completely inhibited by 2.0 mM BQ, indicating the existence of $O_2^{\bullet-}$ in this ECL system. But the ECL intensity was hardly suppressed when 2.0 mM IPA was added, indicating that little •OH was generated. On this basis, a possible mechanism of this ECL system was depicted in Fig. 5C and described as follows in detail.

Decisive steps: $O_2 + e^- \rightarrow O_2^{\bullet-}$ (1)

$$\text{Fe(II)-N-C} - e^- \rightarrow \text{Fe(III)-N-C} \quad (2)$$

ECL emission: $LH^- - e^- \rightarrow L^{\bullet-} + H^+$ (3)

$$L^{\bullet-} + O_2^{\bullet-} \rightarrow LO_2^{2-} \quad (4)$$

$$LO_2^{2-} \rightarrow AP^{2-*} + N_2 \quad (5)$$

$$AP^{2-*} \rightarrow AP^{2-} + h\nu \quad (6)$$

First, dissolved O_2 was reduced to $O_2^{\bullet-}$ by the electrocatalyst modified on GCE when the cycle scan starts from 0 to -0.4 V, and it was the decisive step. Meanwhile, the cathodoluminescence of luminol was excited by $O_2^{\bullet-}$ slightly, which was even negligible. Luminol anions (LH^-) were then electrochemically oxidized to luminol anionic radicals ($L^{\bullet-}$) upon anodic potential scanning. Finally, $L^{\bullet-}$ reacted with accumulated $O_2^{\bullet-}$ to form excited-state 3-aminophthalate anion (AP^{2-*}), thus enormously boosted the ECL and realized signal amplification.

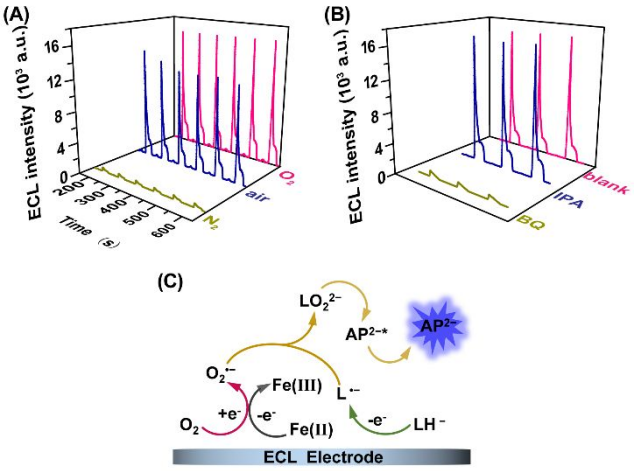

Figure 5 (**A**) ECL-time curves of Fe-N-C-800/luminol/GCE under O_2, air, N_2 saturated atmosphere in 4.0 mL of 0.1 M, pH 11 PBS solution. (**B**) ECL intensity variation with addition of 2 mM IPA and BQ as radical scavengers. (**C**) Possible ECL mechanism of the proposed Fe-N-C/luminol system.

ECL quenching mechanism of luminol/Fe-N-C by TC. As we observed, the ECL of luminol/Fe-N-C decayed with the increase of TC concentration, and a competition mechanism can be derived. As far as we know, it has been reported that

TC can be effectively oxidized by singlet oxygen and hydroxyl radical.[24] In this system, as noted above, $O_2^{\bullet-}$ was the main active species for TC degradation. Therefore, the ECL quenching mechanism was highly possible to attribute to the reaction between TC and the oxidizing intermediate $O_2^{\bullet-}$. Amount of $O_2^{\bullet-}$ was quickly consumed by TC before it reached the anode potential, so that TC can effectively hinder the ECL process since few remaining $O_2^{\bullet-}$ can react with luminol anionic radicals.

■ CONCLUSION

In summary, highly efficient Fe-N-C catalyst for O_2 activation was successfully synthesized by rational choice of bridging ligand and well control of pyrolysis to fit in ECL system as a coreactant accelerator. And a highly efficient mechanistic path for ECL signal amplification with coreactant generating *in situ* was successfully established and clarified. The ECL was drastically enhanced *via* generating abundant $O_2^{\bullet-}$ radicals *in situ* and decreasing the transferring distance of radicals. Effects of pyrolysis on coordination environment and electronic structure of active sites in Fe-N-C were well characterized, looking forward to inspiring a basic understanding of the potential structure-activity relationship. The remarkable performance of the proposed ECL biosensor was confirmed by sensitive detection of TC antibiotic, clarifying a promising application prospect of the proposed ECL amplification strategy in biological analysis and environmental monitoring. Although this Fe-N-C/luminol-based systems show excellent ECL performance, it is still worth exploring more analytical applications of the proposed ECL amplification strategy and further developing other non coreactant ECL systems.

ASSOCIATED CONTENT

Supporting Information

The Supporting Information is available free of charge on the ACS Publications website.

AUTHOR INFORMATION

Corresponding Author

* Dan Shan — School of Environmental and Biological Engineering, Nanjing University of Science and Technology, Nanjing 210094, China;
E-mail: danshan@njust.edu.cn

Author Contributions

All authors have given approval to the final version of the manuscript.

Li-Ping Zong: Data curation, Investigation, Formal analysis, Methodology, Writing-original draft.

Junji Li, Guofang Shu and Robert-S. Marks: Conceptualization, Formal analysis, Writing-review.

Xue-Ji Zhang, Serge Cosnier and Dan Shan: Conceptualization, Formal analysis, Funding acquisition, Methodology, Project administration, Writing-review and editing.

Notes

The authors declare no competing financial interests.

ACKNOWLEDGMENT

This research was supported by the National Natural Science Foundation of China (Nos. 21675086 and 62001224), the Natural Science Foundation of Jiangsu Province (No. BK20190457), the 69th batch of China Postdoctoral Science Foundation (No. 2021M691600), the Fundamental Research Funds for the Central Universities (Nos. 30918012202 and 30919011213), "Overseas Academic Partnership Program" of Nanjing University of Technology (2019), and a project founded by the priority academic program development of Jiangsu Higher Education Institutions (PAPD). The authors wish also to acknowledge the support from the Sino-French international research network "New nanostructured materials and biomaterials for renewable electrical energy sources" for providing facilities.

REFERENCES

(1) Ahmad, F.; Zhu, D.; Sun, J. *Environ. Sci. Eur.* **2021**, *33*.

(2) Zhang, X. P.; Chandra, A.; Lee, Y. M.; Cao, R.; Ray, K.; Nam, W. *Chem. Soc. Rev.* **2021**, *50*, 4804-4811.

(3) Keshari, K.; Bera, M.; Velasco, L.; Munshi, S.; Gupta, G.; Moonshiram, D.; Paria, S. *Chem. Sci.* **2021**, *12*, 4418-4424.

(4) Marshall-Roth, T.; Libretto, N. J.; Wrobel, A. T.; Anderton, K. J.; Pegis, M. L.; Ricke, N. D.; Voorhis, T. V.; Miller, J. T.; Surendranath, Y. *Nat. Commun.* **2020**, *11*, 5283.

(5) Lefèvre, M., Proietti, E., Jaouen, F., Dodelet, J. P. *Sci.* **2009**, *324*, 71-74.

(6) Zhao, C. X.; Li, B. Q.; Liu, J. N.; Zhang, Q. *Angew. Chem. Int. Ed. Engl.* **2021**, *60*, 4448-4463.

(7) Williams, N. J.; Dean, N. E.; VanDerveer, D. G.; Luckay, R. C.; Hancock, R. D. *Inorg. Chem.* **2009**, *48*, 7853-7863.

(8) Li, Z. Z.; Wu, M. X.; Ding, S. N. *Anal. Methods* **2021**, *13*, 2297-2304.

(9) Gan, Z.; Hu, X.; Xu, X.; Zhang, W.; Zou, X.; Shi, J.; Zheng, K.; Arslan, M. *Food Chem.* **2021**, *354*, 129501.

(10) Alipour, M.; Akintola, O.; Buchholz, A.; Mirzaei, M.; Eshtiagh-Hosseini, H.; Görls, H.; Plass, W. *Eur. J. Inorg. Chem.* **2016**, *2016*, 5356-5365.

(11) Mirzaei, M.; Eshtiagh-Hosseini, H.; Hassanpoor, A. *Inorg. Chim. Acta* **2019**, *484*, 332-337.

(12) Liu, W.; Zhang, L.; Liu, X.; Liu, X.; Yang, X.; Miao, S.; Wang, W.; Wang, A.; Zhang, T. *J. Am. Chem. Soc.* **2017**, *139*, 10790-10798.

(13) Li, J.; Ghoshal, S.; Liang, W.; Sougrati, M.-T.; Jaouen, F.; Halevi, B.; McKinney, S.; McCool, G.; Ma, C.; Yuan, X.; Ma, Z.-F.; Mukerjee, S.; Jia, Q. *Energy Environ. Sci.* **2016**, *9*, 2418-2432.

(14) Zhu, Y.; Zhang, B.; Liu, X.; Wang, D. W.; Su, D. S. *Angew. Chem. Int. Ed. Engl.* **2014**, *53*, 10673-10677.

(15) Tan, X.; Liu, S.; Liu, Y.; Gu, Y.; Zeng, G.; Cai, X.; Yan, Z.; Yang, C.; Hu, X.; Chen, B. *Sci. Rep.* **2016**, *6*, 39691.

(16) Yan, X.; Xu, X.; Liu, Q.; Guo, J.; Kang, L.; Yao, J. *Electrochim. Acta* **2018**, *389*, 260-266.

(17) Zhang, W.; Feng, Y. Q. *Acta Crystallogr. C* **2014**, *70*, 562-565.

(18) Zhuang, Y.; Liu, Q.; Kong, Y.; Shen, C.; Hao, H.; Dionysiou, D. D.; Shi, B. Environ. Sci.-Nano. **2019**, *6*, 388-398.

(19) Zong, L. P.; Ruan, L. Y.; Li, J.; Marks, R. S.; Wang, J. S.; Cosnier, S.; Zhang, X. J.; Shan, D. *Biosens. Bioelectron.* **2021**, *184*, 113216.

(20) Lin, L.; Zhu, Q.; Xu, A. W. *J. Am. Chem. Soc.* **2014**, *136*, 11027-11033.

(21) Guo, J.; Yan, X.; Liu, Q.; Li, Q.; Xu, X.; Kang, L.; Cao, Z.; Chai, G.; Chen, J.; Wang, Y.; Yao, J. *Nano. Energy* **2018**, *46*, 347-355.

(22) Xue, F.; Liu, X.; Liu, J. *J. Phys. Chem. C* **2018**, *123*, 684-690.

(23) Kramm, U. I.; Herrmann-Geppert, I.; Behrends, J.; Lips, K.; Fiechter, S.; Bogdanoff, P. *J. Am. Chem. Soc.* **2016**, *138*, 635-640.
(24) Qu, J.; Ge, Y.; Zu, B.; Li, Y.; Dou, X. *Small* **2016**, *12*, 1369-1377.
(25) Ji, Q.; Bi, L.; Zhang, J.; Cao, H.; Zhao, X. S. *Energy Environ. Sci.* **2020**, *13*, 1408-1428.
(26) Gong, L.; Zhang, H.; Wang, Y.; Luo, E.; Li, K.; Gao, L.; Wang, Y.; Wu, Z.; Jin, Z.; Ge, J.; Jiang, Z.; Liu, C.; Xing, W. *Angew. Chem. Int. Ed. Engl.* **2020**, *59*, 13923-13928.
(27) Xiao, M.; Chen, Y.; Zhu, J.; Zhang, H.; Zhao, X.; Gao, L.; Wang, X.; Zhao, J.; Ge, J.; Jiang, Z.; Chen, S.; Liu, C.; Xing, W. *J. Am. Chem. Soc.* **2019**, *141*, 17763-17770.
(28) Yan, X.; Xu, X.; Zhong, Z.; Liu, J.; Tian, X.; Kang, L.; Yao, J. *Electrochim. Acta* **2018**, *281*, 562-570.
(29) Lau, C.; Lu, J.; Kai, M. *Anal. Chim. Acta* **2004**, *503*, 235-239.

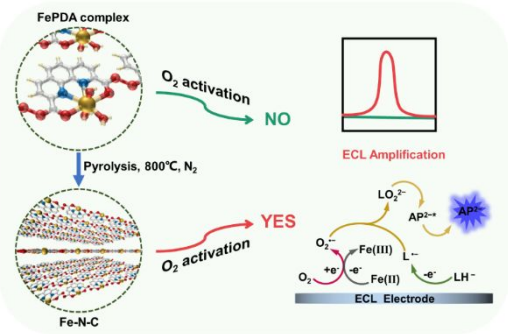

Table of Contents artwork